

A nonlinear elastic instability in channel flows at low Reynolds numbers

L. Pan¹, A. Morozov², C. Wagner³, and P. E. Arratia^{1*}

¹*Department of Mechanical Engineering and Applied Mechanics, University of Pennsylvania, Philadelphia, USA*

²*SUPA, School of Physics and Astronomy, University of Edinburgh, Edinburgh, UK and*

³*Experimental Physics, Saarland University, Saarbrücken, DE*

(Dated: June 4, 2019)

It is presently believed that flows of viscoelastic polymer solutions in geometries such as a straight pipe or channel are linearly stable. Here we present experimental measurements that point to the contrary. We perform particle-tracking velocimetry in a long, straight microfluidic channel where we perturb the flow by placing a variable number of obstacles at the channel entrance. Above a critical flow rate and a critical size of the perturbation, a sudden onset of large velocity fluctuations indicates presence of a subcritical instability. Together with the previous observations of hydrodynamic instabilities in curved geometries, our results suggest that any flow of polymer solutions becomes unstable at sufficiently high flow rates.

PACS numbers: 47.50.-d, 47.20.Gv, 61.25.he

Solutions containing polymer molecules do not flow like water. Even when flowing slowly, these fluids can exhibit hydrodynamic instabilities [1–8] and a new type of turbulence - the so-called *purely elastic turbulence* [9, 10] even at low Reynolds numbers (Re). These phenomena, driven by the anisotropic elasticity of the fluid, were experimentally observed only in geometries with sufficient curvature, like rotational flows between two cylinders [1, 11, 12] and plates [13], in curved channels [10, 14], and around obstacles [15]. Most of the nonlinear flow behavior observed in these studies arises from the extra elastic stresses due to the presence of polymer molecules in the fluid. These elastic stresses are history dependent and evolve on the time-scale λ that in dilute solutions is proportional to the time needed for a polymer molecule to relax to its equilibrium state [16].

A common feature of the above-mentioned geometries is the presence of curved streamlines in the base flow with a sufficient velocity gradient across the streamlines. It has been argued that this is a necessary condition for infinitesimal perturbations to be amplified by the normal stress imbalances in viscoelastic flows [1, 8, 13]. This condition can be written as $(\lambda UN_1)/(R\Sigma) \geq M$ [8, 13, 17], where M is a constant that only depends on the type of flow geometry, U is a typical velocity along the streamlines, R is the radius of streamline curvature, and N_1 and Σ are the first normal stress difference and the shear stress, correspondingly. According to this condition, purely elastic *linear* instabilities are not possible when the curvature of the flow geometry is zero, and infinitesimal perturbations decay at a rate proportional to $1/\lambda$ [8, 18, 19]. This statement has often been misinterpreted to imply general stability of viscoelastic parallel shear flows, like flow in a straight pipe or channel, under arbitrary flow perturbations. Recent theoretical [17, 20, 21] and indirect experimental [22, 23] evidence, however, points towards a nonlinear instability in flows

with parallel streamlines even at low Re . Here, we experimentally prove the existence of such instability.

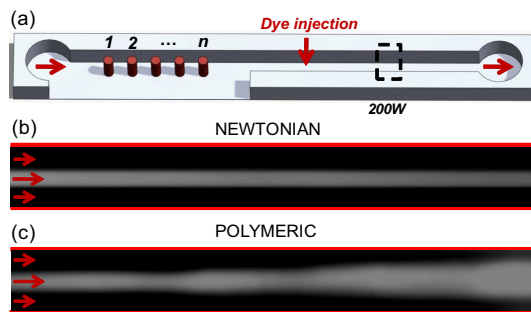


FIG. 1. Color Online. (a) Sketch of experimental setup showing a long microchannel ($90 \mu\text{m}$ deep, $100 \mu\text{m}$ wide and 3.3 cm long) comprised of an initial perturbation region ($\sim 0.3 \text{ cm}$ long) with cylinders ($d = 50 \mu\text{m}$) followed by a long parallel shear region ($\sim 3 \text{ cm}$). The dash line window represents a typical sampling position. (b, c) Sample snapshots of dye advection visualization experiments at $Re < 0.01$ and $n=15$, where n is the number of cylinders. Dye is injected at approximately 1.0 cm downstream from the end of the initial perturbation region. Snapshots correspond to flow patterns in the parallel flow region. (b) Newtonian case: the snapshot shows a very stable stream of dyed fluid that only mixes due to molecular diffusion. (c) Polymeric case ($Wi=10.9$): the dye patterns show a stream that quickly broadens and mixes with undyed fluid. Field of view is only nine channel widths.

Experiments are performed in a long, straight microchannel that consists of a short initial perturbation region followed by a long parallel flow region (Fig. 1a). The channels are $90 \mu\text{m}$ deep, $100 \mu\text{m}$ wide and 3.3 cm long. The perturbation region is very short ($\sim 0.3 \text{ cm}$) and contains evenly-spaced cylinders that are $50 \mu\text{m}$ in diameter and $90 \mu\text{m}$ tall; the distance between two adjacent cylinders is $200 \mu\text{m}$ (center to center). The number of cylinders n in this region varies from 1 to 15, in which the goal is to introduce finite amplitude disturbances into the flow; a channel devoid of cylinders $n=0$ is also used

* parratia@seas.upenn.edu

for control. The parallel flow region is a long (~ 3.0 cm), straight channel devoid of cylinders in which the fate of an initial disturbance is monitored using dye advection and velocimetry methods. All microchannels are fabricated using standard soft-lithography methods [24].

Both Newtonian and polymeric fluids are investigated. The Newtonian fluid is a 90% by weight glycerol aqueous solution with shear viscosity of approximately 0.2 Pa·s. The polymer used here is high molecular weight polyacrylamide (PAA, 18×10^6 MW), which has a flexible backbone. The polymeric solution is made by adding 300 ppm of PAA to a viscous Newtonian solvent (90% by weight glycerol aqueous solution). Both fluids are characterized using a strain-controlled rheometer at 23 °C [25]. For all experiments, the Reynolds number (Re) is small (<0.01) due to the channel small length scale and high fluid viscosity. Here $Re = \rho UL/\eta$, where U is the fluid velocity, L is a characteristic length scale, ρ is the fluid density, and η is the fluid viscosity. The magnitude of the elastic stresses compared to viscous stresses is characterized by the Weissenberg number [26, 27] defined as $Wi = N_1/(2\dot{\gamma}\eta)$, where N_1 is the first normal stress difference and $\dot{\gamma}$ is the shear-rate. Please see [25] for further details.

Two main types of experiments are performed: dye advection and particle tracking velocimetry. Dye advection experiments are performed by injecting small amounts of fluorescein at the center of the channel from the top using a multilayer injection scheme (Fig. 1a). Dyed fluid is injected at approximately 1.0 cm downstream from the initial perturbation region in order to display only the flow patterns in the parallel flow region after the perturbation is introduced. Images are taken 1 cm downstream from injection point. Figures 1(b) and (c) show snapshots of the dye advection experiments at $Re < 10^{-2}$ for both the Newtonian and polymeric cases, respectively for a channel containing 15 cylinders ($n = 15$). The Newtonian case (Fig. 1b) shows a stable layer of dyed fluid that does not mix with the undyed fluid except by diffusion. An entirely different pattern is observed when the Newtonian fluid is replaced by a polymeric solution at $Wi = 10.9$ (Fig. 1c). The dyed fluid quickly mixes with the undyed fluid, which suggests the presence of hydrodynamic instabilities and time-dependent flow. Below we show that this time-dependent flow is not due to the downstream advection of the fluctuations around the cylinders, but rather is a unique non-linear state independent of the original perturbation.

Particle velocimetry methods are used to quantify the instability observed in the dye experiments. The flow is seeded with small fluorescent particles ($0.86 \mu\text{m}$ in diameter) that are tracked using a CMOS camera operated at 3 kHz and an epi-fluorescent microscope. The particle tracks are measured at a mid-point between the top and bottom plates of the channel in order to minimize the effects of out-of-plane velocity gradients; the thickness of the measuring plane is approximately $2 \mu\text{m}$. The measured particle tracks are used to compute the flow

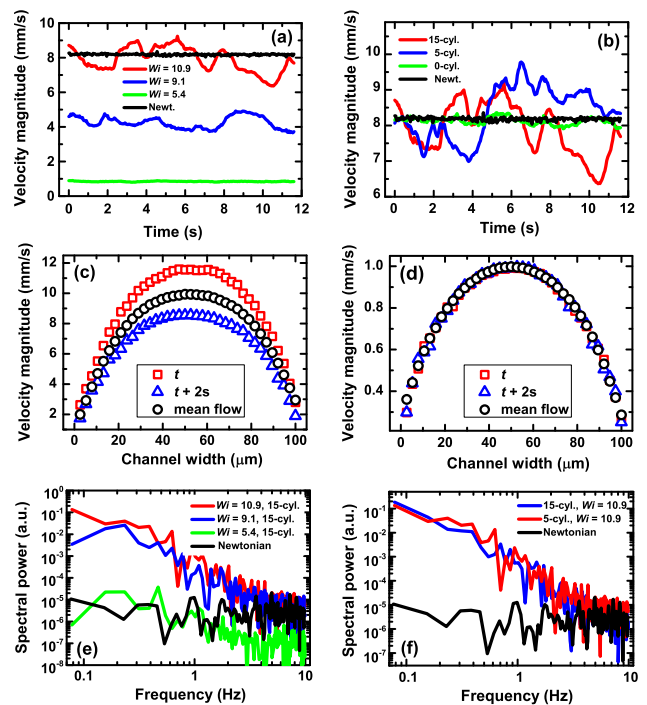


FIG. 2. Color Online. Velocity signals, profiles and corresponding power spectra. (a,b) Spatially averaged velocity magnitude as a function of time measured in the parallel flow region $200W$ (or 2 cm) downstream from the last cylinder, where $W = 100 \mu\text{m}$, for (a) $n=15$ as a function of Wi and for (b) $Wi=10.9$ as a function of n . The polymeric fluid flow becomes time-dependent under a sufficiently large initial perturbation. The straight channel case ($n=0$) shows no velocity fluctuations under the same conditions and even for the highest value of Wi (250 s^{-1}). No fluctuations are found for the Newtonian case at any flow rate. (c,d): Instantaneous and mean streamwise velocity profiles as a function of the cross-channel coordinate for $n=15$ for (c) $Wi = 5.4$ and (d) $Wi = 10.9$. The velocity profiles are computed at time intervals of 2 s and are compared to their time-averaged mean profile. (e,f): Corresponding power spectra of the velocity measurements for (a) and (b) respectively, showing a 2-4 orders of magnitude increase in the spectral power at low frequencies.

velocity fields. Measurements are performed in several locations along the channel including one channel width ($1W$) after the last cylinder as well as $50W$, $100W$, $150W$, and $200W$. The $1W$ measuring location is used to monitor the amplitude of the initial disturbance introduced in the flow by the array of n cylinders. The other measuring locations are used to monitor the fate of the initial disturbance in the parallel flow region.

To quantify the time dependence of the flow, we sample a square area (about 35% of the channel width centered at midpoint) of the velocity fields, and measure the average speed as a function of time. The sampling rates are long enough (~ 1 ms) to ensure the accuracy of the velocimetry measurement but are much shorter than the typical time scale of the fluid motion. All mea-

measurements shown in Fig. 2 are taken at 200W or 2 cm downstream from the last cylinder. Figure 2(a) shows samples of the velocity magnitude records measured far downstream (200W) for a channel with $n=15$ as function of Wi or equivalently flow rate. We find that, for the polymeric case, the velocity fluctuations become larger as Wi is increased. The Newtonian case, on the other hand, produces no such fluctuations at comparable shear-rates (210 s^{-1}). In Fig. 2(b), we show velocity records of the polymeric solution at a fixed $Wi=10.9$ for channels with different number of cylinders n . For the case of an empty channel ($n=0$), the viscoelastic case shows no significant fluctuations even at the highest shear-rate. Time-dependent velocity fluctuations, however, become apparent as cylinders are introduced in the channel. This is further illustrated by plotting the instantaneous and mean velocity profiles of the polymeric fluid. For $Wi=5.4$ (Fig. 2c), there is no time-dependence while for $Wi=10.9$ (Fig. 2d), the instantaneous velocity profiles show significant differences between each other and with the mean profile. Importantly, the amplitude of velocity fluctuations is roughly independent of n at a fixed Wi , as can be seen from Fig. 2(b).

The corresponding power spectra of the velocity signals in Fig. 2(a) and (b) are shown in Fig. 2(e) and (f), respectively. Since the entire velocity field must be measured at each instant, the records are only a few hundred points long, but this is sufficient to establish the qualitative features of the spectra. In Fig. 2(e), we note that the spectral power at low frequencies grows by 2-4 orders of magnitude as the Wi is increased at a fixed n . A similar behavior is observed as n is increased at a fixed Wi . The velocity fluctuations are non-periodic, with a possible power-law spectral decay, indicating that the flow is excited at many time-scales. Such decay has been observed in many flow geometries with curved streamlines and has been interpreted as evidence of elastic turbulence [9, 10]. The Newtonian and $n=0$ (polymeric) cases, on the other hand, show a relatively flat power spectra consistent with noise.

Next, we investigate how the amplitude of the velocity fluctuations changes along the channel. In Fig. 3, we plot the standard deviation σ of the velocity signal normalized by its mean $\langle V \rangle$ measured at different locations in the parallel shear region as function of Wi for $n=15$. As expected, the velocity fluctuations for the Newtonian case are small (~ 0.01) and independent of the channel position even at high shear-rates. Results for the polymeric solution show a different behavior. For Wi up to 5.4, the values of $\sigma/\langle V \rangle$ are relatively large immediately after the last cylinder (1W) due to a well-known instability that develops in the wake of a cylinder for viscoelastic flows at low Re [7, 28]. In our experiments this instability sets in at $Wi \approx 3.5$. However, the velocity fluctuations decay to values close to the Newtonian case in just a few channel widths. This indicates that any flow disturbance that initially develops in the channel is short-lived and damped by viscous forces, and the flow far downstream

is stable for $Wi < 5.4$.

An entirely different behavior emerges for $Wi > 5.4$ and $n=15$. The velocity fluctuations, created in the wake of the array of cylinders, settle to values of $\sigma/\langle V \rangle$ that are significantly larger than the Newtonian case as shown in Fig. 3. These velocity fluctuations decay to only 8-10% after 50W, and remain approximately constant thereafter even at 200W. Similar behavior in $\sigma/\langle V \rangle$ is observed down to $Wi > 8.1$. This data strongly suggests that a time-dependent flow can be created and sustained in the parallel shear flow region of the channel provided the Weissenberg number and the strength of the initial perturbation supplied by the flow around cylinders are both sufficiently large.

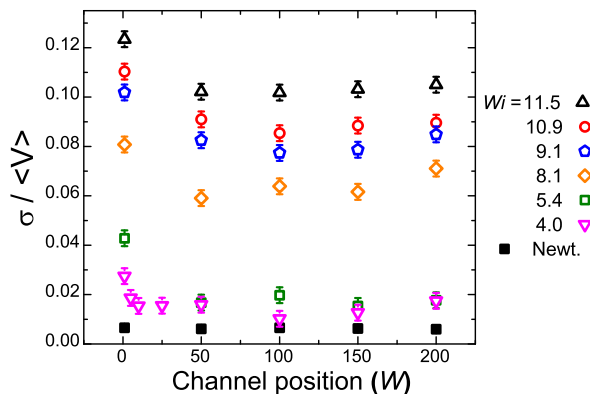


FIG. 3. Color Online. Normalized standard deviation of velocity signals along the parallel flow region as a function of channel position and Wi . The measuring positions are 1W, 50W, 100W, 150W, and 200W downstream from the last cylinder where $W=100 \mu\text{m}$. The 1W location is used to monitor the amplitude of the initial disturbance, while the other locations are used to monitor the fate of the initial disturbance in the parallel flow region. The figure shows the velocity standard deviation σ normalized by its respective mean velocity $\langle V \rangle$ for Wi ranging from 0 (Newtonian) to 11.5. Velocity fluctuations are sustained far downstream in the parallel flow region above a certain Wi , and grows non-linearly as Wi is increased. The normalized standard deviation for the Newtonian fluid is always below 1%, even for the highest shear-rate (250.0 s^{-1}), and shows the absence of velocity fluctuation.

We now study how large a perturbation should be to destabilize the flow. In Fig.4(a), we plot the magnitude of the velocity fluctuations far downstream from the last cylinder as a function of Wi for channels with different number of cylinders n . For $n=0$, no instability is found anywhere in the channel, and the values of $\sigma/\langle V \rangle$ remain near 1%. For $n=1$, a relatively small levels of fluctuations are observed ($\sim 2.5\%$) even for large Wi . The small velocity fluctuations can be a result of pure convection in the sense that part of the velocity fluctuations observed in the wake of the cylinders is convected downstream by the flow [7].

A notable difference in flow behavior is observed when the number of obstacles is further increased. For $n=2$

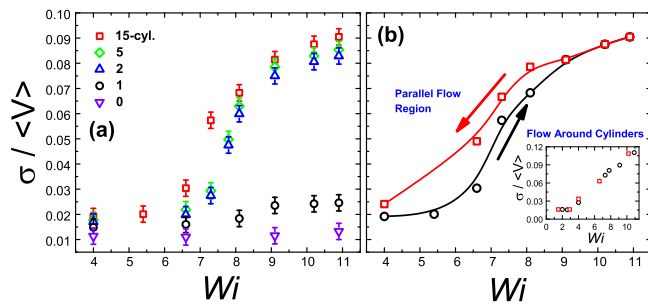


FIG. 4. Color Online. Normalized standard deviation of velocity signals for the polymeric fluid as a function of Wi for channels with different number of cylinders n . All data presented here are measured at $200W$ downstream from the last cylinder. (a) The quantity $\sigma / \langle V \rangle$ showing a clear difference between the lower and higher branches which strongly suggests the existence of non-linear elastic instability in parallel shear flows even at low Re for polymeric fluids. (b) The quantity $\sigma / \langle V \rangle$ as a function of Wi for $n=15$ as the shear-rate is increased (dark curve) and decreased (red curve) shows hysteretic behavior typical of subcritical instabilities. The time interval between each experiment is approximately 1 minute. Lines are added to guide the eye. (Inset) Forward bifurcation diagram for the instability around the cylinders; no hysteresis is observed.

and $Wi < 5.4$, the values of $\sigma / \langle V \rangle$ are still relatively small ($\sim 2\%$). However, for $Wi > 5.4$, the velocity fluctuations sharply increase and reach an asymptotic value of about 9% for large Wi . Similar behavior to the $n=2$ case is observed for the $n=5$ and $n=15$ cases in polymer solutions. The data in Fig 4(a) clearly shows the development of two branches after a critical value of Wi , one in which the flow is stable ($n < 2$) and the other in which the flow is unstable ($n \geq 2$). Importantly, for $n \geq 2$ the level of fluctuations does not depend on n suggesting that the flow has reached the same nonlinear state independent of the initial perturbation. The transition to this state is hysteretic as can be seen from Fig. 4(b):

upon the increase or decrease of the flow rate, the level of fluctuations sharply rises and falls at different Wi 's, which is a typical signature of a subcritical bifurcation. At the same time, the flow around the cylinders, Fig.4(b, inset) shows no hysteresis and no secondary instabilities seem to take place when the flow downstream starts to exhibit an instability. This ultimately proves that, while the cylinders or obstacles play an important role in providing strong initial perturbations to the flow, the resulting bulk instability in the parallel shear flow section of the channel is clearly distinct from the instability around the cylinders.

In summary, we have shown experimentally the existence of a nonlinear subcritical instability for polymeric fluids in a parallel shear flow in the absence of inertia (low Re). The critical value of Wi for the onset of the subcritical instability in the parallel flow is larger than 5.2 for the type of disturbances introduced here. This critical value may, however, be very sensitive to the type and strength of the initial perturbation, and will be further investigated. A possible mechanism leading to this subcritical instability has been proposed [21] in which the initial finite amplitude disturbance produces a new effective base flow with curved streamlines in the parallel flow region and becomes linearly unstable [5, 8]. The transition then would depend on whether the disturbance is sufficiently strong and long-lived to become unstable. This scenario is akin to the transition from laminar to turbulent flow of Newtonian fluids in pipe and channel flows, except that the instability is caused by the nonlinear elastic stresses and not inertia [29, 30].

We thank W. van Saarloos, R. Poole, A. Lindner, and D. Bartolo for engaging discussions and comments on the manuscript. We also thank R. Sureshkumar, M. Graham, R. Larson, B. Khomami, and M. Shatz for fruitful discussions and X. Shen for assistance with rheology. AM acknowledges support from the EPSRC Career Acceleration Fellowship (grant EP/I004262/1). PEA acknowledges partial support from NSF-Career Award CBET-0954084.

-
- [1] R. G. Larson, E. S. G. Shaqfeh, and S. J. Muller, *J. Fluid Mech.* **218**, 573 (1990).
[2] E. S. G. Shaqfeh, *Annu. Rev. Fluid Mech.* **28**, 129 (1996).
[3] R. G. Larson, *Rheol. Acta* **31**, 213 (1992).
[4] P. E. Arratia, C. C. Thomas, J. Diorio, and J. P. Gollub, *Phys. Rev. Lett.* **96**, 144502 (2006).
[5] A. Groisman, M. Enzelberger, and S. R. Quake, *Science* **300**, 955 (2003).
[6] R. J. Poole, M. A. Alves, and P. J. Oliveira, *Phys. Rev. Lett.* **99**, 164503 (2007).
[7] G. H. McKinley, R. C. Armstrong, and R. A. Brown, *Phil. Trans. Roy. Soc. Lond. A* **344**, 265 (1993).
[8] P. Pakdel and G. H. McKinley, *Phys. Rev. Lett.* **77**, 2459 (1996).
[9] A. Groisman and V. Steinberg, *Nature* **405**, 53 (2000).
[10] A. Groisman and V. Steinberg, *New J. of Physics* **6**, 29 (2004).
[11] A. Groisman and V. Steinberg, *Phys. Fluids* **10**, 2451 (1998).
[12] S. J. Muller, R. G. Larson, and E. S. G. Shaqfeh, *Rheol. Acta* **28**, 499 (1989).
[13] G. H. McKinley, P. Pakdel, and A. Oztekin, *J. Non-Newt. Fluid Mech.* **67**, 19 (1996).
[14] A. Groisman and V. Steinberg, *Nature* **410**, 905 (2001).
[15] K. Arora, R. Sureshkumar, and B. Khomami, *J. Non-Newt. Fluid Mech.* **108**, 209 (2002).
[16] R. G. Larson, *The structure and rheology of complex fluids* (Oxford University Press, 1999).
[17] A. N. Morozov and W. van Saarloos, *Physics Reports* **447**, 112 (2007).
[18] T. C. Ho and M. M. Denn, *J. Non-Newt. Fluid Mech.* **3**, 179 (1977).

- [19] H. Wilson, M. Renardy, and Y. Renardy, *J. Non-Newtonian Fluid Mech.* **80**, 251 (1999).
- [20] B. Meulenbroek, C. Storm, A. N. Morozov, and W. van Saarloos, *J. Non-Newtonian Fluid Mech.* **116**, 235 (2004).
- [21] A. N. Morozov and W. van Saarloos, *Phys. Rev. Lett.* **95**, 024501 (2005).
- [22] V. Bertola and et al., *Phys. Rev. Lett.* **90**, 114502 (2003).
- [23] D. Bonn, F. Ingremeau, Y. Amarouchene, and H. Kellay, *Phys. Rev. E* **84**, 045301 (2011).
- [24] J. C. McDonald and G. M. Whitesides, *Acc. Chem. Res.* **35**, 491 (2002).
- [25] See supplementary material.
- [26] J. J. Magda and et al., *Macromolecules* **26**, 1696 (1993).
- [27] R. B. Bird, *Dynamics of Polymeric Liquids: Fluid Mechanics*, 2nd ed., Vol. 1 (Wiley, New York, 1987).
- [28] D. F. James and A. J. Acosta, *J. Fluid Mech.* **42**, 269 (1970).
- [29] B. Hof and et al., *Science* **305**, 1594 (2004).
- [30] K. Avila and et al., *Science* **333**, 192 (2011).